iScience, Volume *23*

Supplemental Information

Propagation of Pathological α-Synuclein from the Urogenital Tract to the Brain Initiates MSA-like Syndrome

Xuebing Ding, Lebo Zhou, Xiaoyi Jiang, Han Liu, Jing Yao, Rui Zhang, Dongxiao Liang, Fengfei Wang, Mingming Ma, Beisha Tang, Erxi Wu, Junfang Teng, and Xuejing Wang

Supplemental Figures

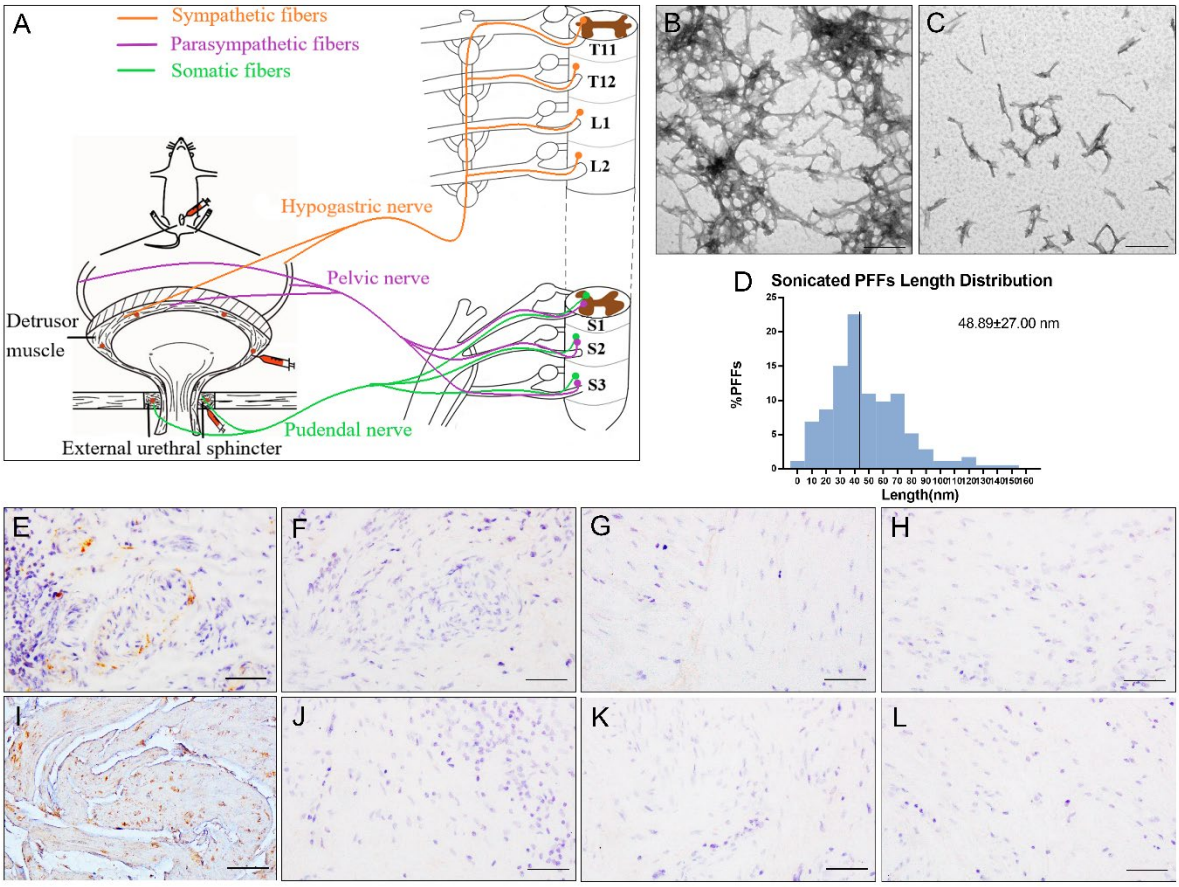

Figure S1. Related to Figure 1 and Transparent Methods. (A) Schematic displaying the innervation of the EUS and DET by the hypogastric, pelvic, and pudendal nerves. (B, C) Representative negative-stained transmission electron micrographs of α-Syn PFFs before sonication (B) and after sonication (C). (D) Histogram representation of >170 sonicated fibrils measured from randomly captured electron microscopy images. Black bars represent group median, with mean and corresponding group standard deviation indicated in bold font. (E-L) Representative immunohistochemical images of DET from MSA (E, I), PD (F, J), PSP (G, K) and NC (H, L) using anti-pα-Syn (Ser129) (E-H) and anti-α-Syn aggregates (5G4) (I-L) antibodies. [Scale bars, 500 nm (B, C); 100 μm (E-L).]

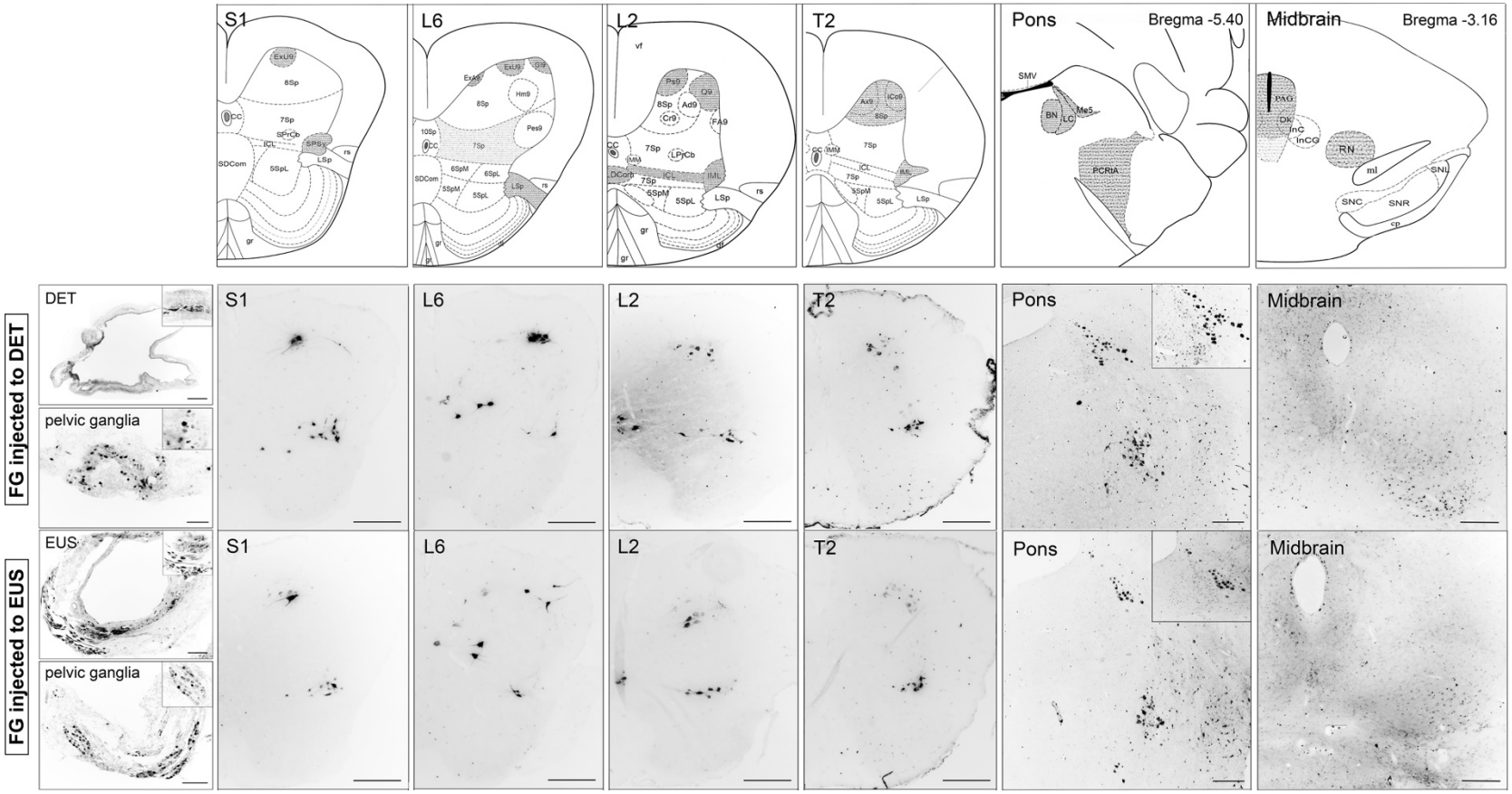
S1
L6
L2
T2
Pons
Bregma -5.40
Midbrain
Bregma -3.16
FG injected to DET
FG injected to EUS
DET
EUS
pelvic ganglia
pelvic ganglia

Figure S2. Representative images of FG-labeled neurons in DET- and EUS-FG C57BL/6 mice. Related to Figure 2. All FG-labeled neurons appeared bilaterally while displayed one side. Schematics in the upper panel displayed the map of retrograde tracing areas (shaded areas) at different levels. Labeling appeared in DET-FG C57BL/6 mice (middle panel) and EUS-FG C57BL/6 mice (lower panel). Insets show a higher magnification relative to the main image. [Scale bars, 200 μm (DET, EUS, pons); 100 μm (pelvic ganglia); 500 μm (S1, L6, L2, T2, midbrain).] Abbreviation: 5SpL: lamina V of the spinal gray, lateral part; 5SpM: lamina V of the spinal gray, medial part; 6SpL: lamina Ⅵ of the spinal gray, lateral part; 6SpM: lamina Ⅵ of the spinal gray, medial part; 7Sp: lamina Ⅶ of the spinal gray; 8Sp: lamina Ⅷ of the spinal gray; 10Sp: lamina Ⅹ of the spinal gray; Ad9: adductor motoneurons of lamina Ⅸ; Ax9: axial muscle motoneurons of lamina Ⅸ; BN: Barrington's nucleus; CC: central canal; cp: cerebral peduncle, basal part; Cr9: cremaster motoneurons of lamina Ⅸ; csc: commissure of the superior colliculus; DET: detrusor; df: dorsal funiculus; Dk: nucleus of Darkschewitsch; dl: dorsolateral fasciculus (Lissauer); ExA9: external anal sphincter motoneurons of lamina IX; ExU9: external urethral sphincter motoneurons of lamina IX; EUS: external urethral sphincter; FG: Fluoro-Gold; Gl9: gluteal motoneurons of lamina IX; gr: gracile fasciculus; Hm9: hamstring motoneurons of lamina Ⅸ; ICL: intercalated nucleus; ICo9: intercostal muscle motoneurons of lamina Ⅸ; IML: intermediolateral columns; IMM: intermediomedial column; InCG: interstitial nucleus of Cajal, greater part; InC: interstitial nucleus of Cajal; LC: locus coeruleus; LDCom: lumbar dorsal commissural nucleus; LPrCb: lumbar precerebellar nucleus; LSp: lateral spinal nucleus; Me5: mesencephalic trigeminal nucleus; ml: medial lemniscus; PAG: periaqueductal gray; PCRtA: parvocellular reticular nucleus alpha; Pes9: pes motoneurons of lamina Ⅸ; Ps9: psoas motoneurons of lamina IX; Q9: quadriceps motoneurons of lamina IX; RN: red nucleus; rs: rubrospinal tract; SDCom: sacral dorsal commissural nucleus; SMV: superior medullary velum; SNC: substantia nigra pars compacta; SNL: substantia nigra, lateral part; SNR: substantia nigra, reticular part; SPrCb: sacral precerebellar nucleus; SPSy: sacral parasympathetic nucleus; vf: ventral funiculus.

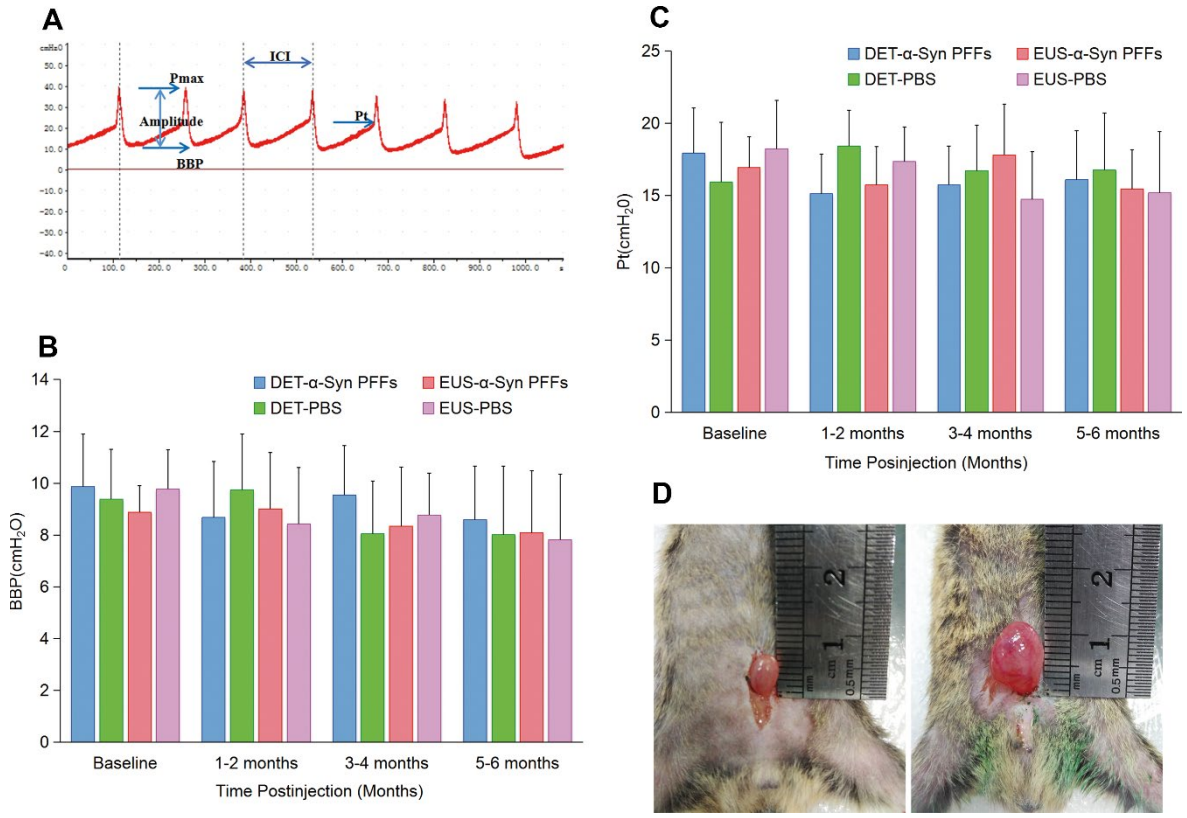

Figure S3. Urinary function analysis. Related to Figure 5. (A) Representative cystometric curve of normal C57BL/6 mice. (B and C) Summary bar graphs from urodynamic evaluation about BBP (B) and Pt (C) for EUS and DET TgM83$^{+/-}$ mice. EUS-α-Syn PFFs TgM83$^{+/-}$ mice n = 18, DET-α-Syn PFFs TgM83$^{+/-}$ mice n = 16, EUS-PBS TgM83$^{+/-}$ mice n = 22, DET-PBS TgM83$^{+/-}$ mice n = 20. Data are the means ± SD. Statistics was performed employing the Student's t test and Mann-Whitney test. (D) Bladder size of EUS-α-Syn PFFs (right) and EUS-PBS (left) TgM83$^{+/-}$ mice at 6-month post-injection (mpi).

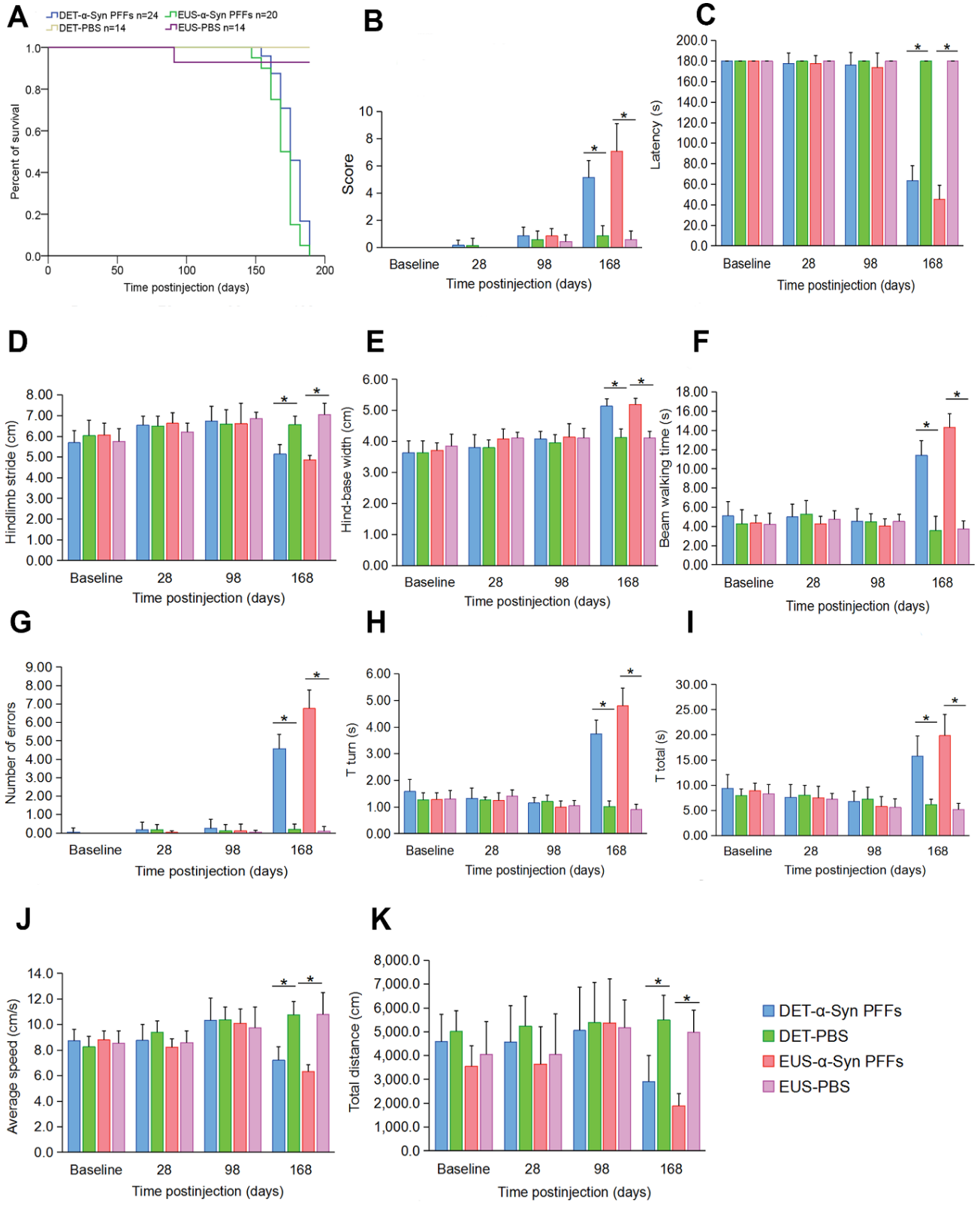
A
DET-α-Syn PFFs n=24
EUS-α-Syn PFFs n=20
DET-PBS n=14
EUS-PBS n=14
Percent of survival
Time postinjection (days)
B
Score
Baseline
28
98
168
Time postinjection (days)
C
Latency (s)
Time postinjection (days)
D
Hindlimb stride (cm)
Time postinjection (days)
E
Hind-base width (cm)
Time postinjection (days)
F
Beam walking time (s)
Time postinjection (days)
G
Number of errors
Time postinjection (days)
H
T turn (s)
Time postinjection (days)
I
T total (s)
Time postinjection (days)
J
Average speed (cm/s)
Time postinjection (days)
K
Total distance (cm)
Time postinjection (days)
DET-α-Syn PFFs
DET-PBS
EUS-α-Syn PFFs
EUS-PBS

Figure S4. Behavioral analysis of TgM83$^{+/-}$ mice. Related to Figure 4 and 5. (A) Kaplan-Meier survival plot shows decreased survival time (due to death or euthanasia because of paralysis) for α-Syn PFFs TgM83$^{+/-}$ mice compared with age-matched PBS TgM83$^{+/-}$ mice. (B) The mean score of MBS. (C) Latency to fall from the rotarod. (D and E) Footprint analysis of the hindlimb stride length (D) and the hind-base width (E). (F and G) The average time to cross the beam (F) and the average number of side slip errors (G) on the beam. (H and I) T turn (H) and T total (I) of the pole test. (J and K) Average speed (J) and total distance (K) traveled during 15 minutes in the open field test. EUS-α-Syn PFFs TgM83$^{+/-}$ mice n = 12, DET-α-Syn PFFs TgM83$^{+/-}$ mice n = 20, EUS-PBS TgM83$^{+/-}$ mice n = 14, DET-PBS TgM83$^{+/-}$ mice n = 14. Data are the means ± SD. Statistical analysis was done by using the Student's t test and Mann-Whitney test, *P < 0.05.

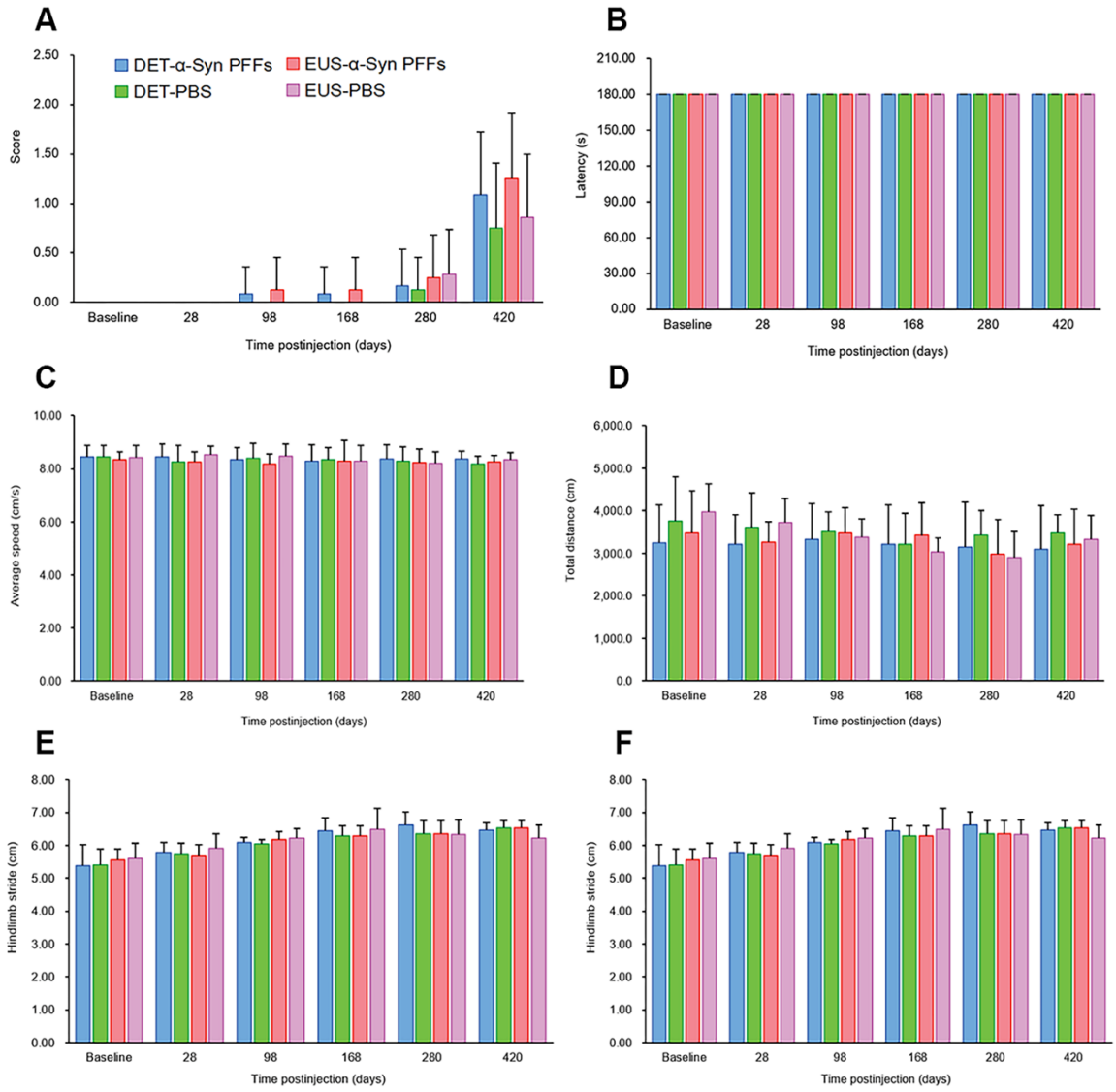

Figure S5. Behavioral analysis of C57BL/6 mice injected with human α-Syn PFFs. Related to Figure 4 and 5. (A) The mean score of MBS. (B) Latency to fall from the rotarod. (C and D) Average speed (C) and total distance (D) traveled during 15 minutes in the open field test. (E and F) Footprint analysis of the hindlimb stride length (E) and the hind-base width (F). EUS-α-Syn PFFs C57BL/6 mice n = 8, DET-α-Syn PFFs C57BL/6 mice n = 12, EUS-PBS C57BL/6 mice n = 7, DET-PBS C57BL/6 mice n = 8. Data are the mean ± SD. Statistical analysis was performed by using the Student's t test and Mann-Whitney test, n.s., non-significant.

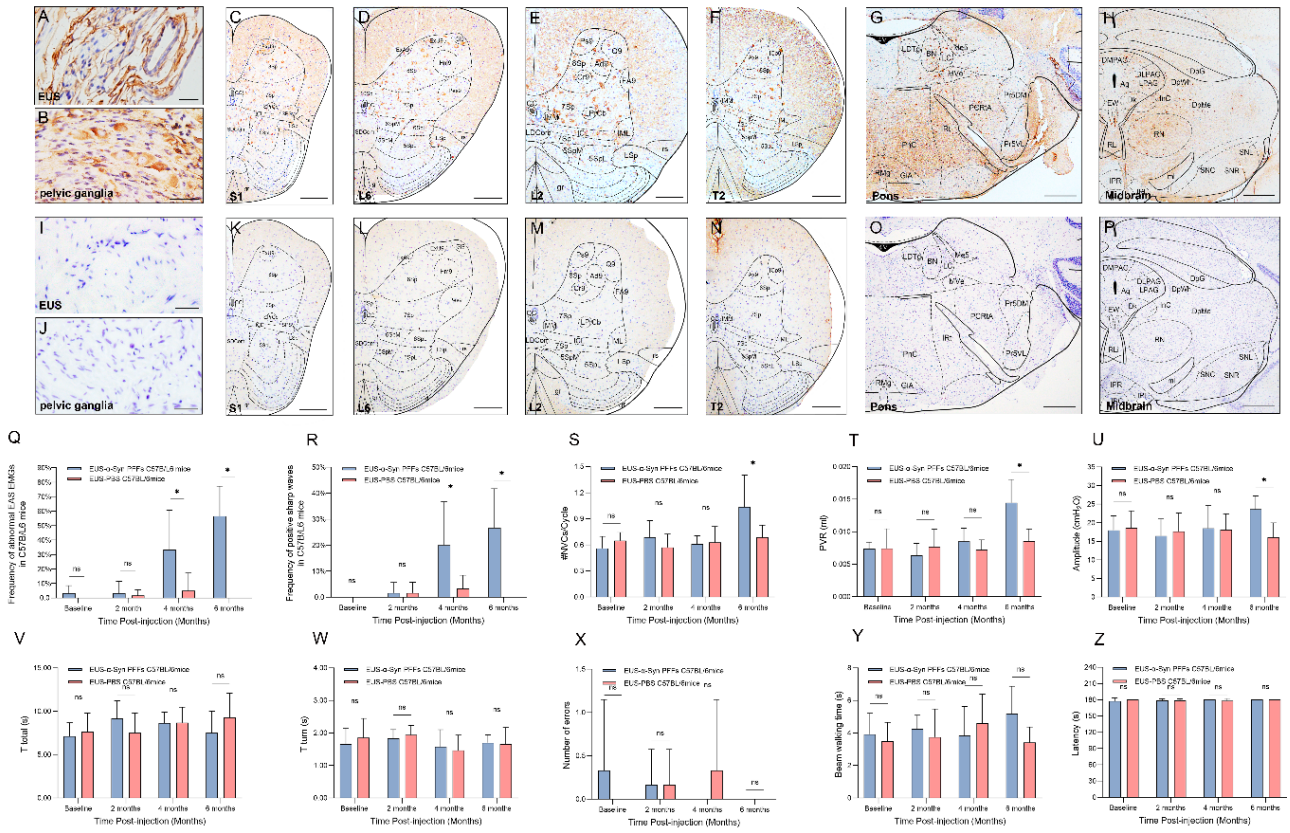

Figure S6. Related to Figure 2. (A-P) Representative immunohistochemical results of different segments from C57BL/6 mice injected with synthetic mouse α-Syn PFFs (A-H) and PBS (I-P) at 6 mpi. Pathological α-Syn was stained with anti-phospho-α-Syn (Ser 129) antibody. Representative images displayed the distribution of pα-Syn in EUS (A, I), pelvic ganglia (B, J), S1 (C, K), L6 (D, L), L2 (E, M), T2 (F, N), pons (G, O), and midbrain (H, P). [Scale bars, 40 μm (A, B, I, J); 250 μm (C-F, K-N); 1 mm (G, H, O, P).] (Q, R) Frequencies of abnormal EAS EMGs (Q) and positive sharp waves (R) in EUS-mouse α-Syn PFFs and PBS C57BL/6 mice. (S-U) Urodynamic evaluation for EUS-mouse α-Syn PFFs and PBS C57BL/6 mice including #NVCs/Cycle (S), PVR (T), and amplitude (U). (V-Z) Behavioral analysis of EUS-mouse α-Syn PFFs and PBS C57BL/6 mice. (V, W) T total (V) and T turn (W) of the pole test. (X, Y) The average number of side slip errors to cross the beam (X) and the average time (Y) on the beam. (Z) Latency to fall from the rotarod. n = 6 animals per group. Data are the means ± SD. Statistics was analyzed employing the Student's t test. *P < 0.05 indicates a significant difference between EUS-mouse α-Syn PFFs groups and PBS groups.

Supplemental Table

Table S1. Characteristics and the exam findings of patients. Related to Figure 1.

Age	Sex	Diagnosis	Duration (year)	MRI	UMSARS				Urodynamic examination†	Perianal electromyography†	α-synuclein filament in the bladder DET‡	α-synuclein filament in EUS§
					UMSARS I	UMSARS II	UMSARS III	UMSARS IV				
54	M	MSA-P	1.5	+	2	5	+	1	+	+	-	0
57	F	MSA-P	8	+	32	50	+	4	+	+	+	0
63	F	MSA-P	2	+	14	18	+	2	-	+	-	0
59	F	MSA-P	4	+	21	18	+	3	-	+	-	0
46	M	MSA-P	2	+	9	14	+	2	+	+	-	0
68	M	MSA-P	7	+	20	31	+	3	+	+	+	0
66	F	MSA-P	<1	+	7	12	+	1	-	+	+	0
70	F	MSA-P	3	+	32	46	+	4	+	+	+	0
66	F	MSA-P	3	+	18	24	+	3	+	+	-	+
72	F	MSA-P	5	+	34	42	+	4	+	+	+	+
63	M	MSA-P	2	+	7	13	+	2	+	-	-	+
64	F	MSA-P	7	+	33	42	+	5	+	+	+	+
59	F	MSA-P	4	+	18	15	+	4	+	-	+	+
59	M	MSA-C	2	+	10	13	+	2	+	+	+	0
50	M	MSA-C	1.5	+	2	3	+	1	-	-	-	0
47	M	MSA-C	8	+	30	21	+	4	+	+	+	0
63	F	MSA-C	2	+	21	14	+	1	+	-	-	0
50	M	MSA-C	2	+	5	6	+	1	+	-	-	0
61	M	MSA-C	3	+	20	18	+	4	+	+	+	0
61	M	MSA-C	5	+	8	9	+	2	+	+	+	0
51	F	MSA-C	3	+	8	6	+	1	-	+	-	0
58	F	MSA-C	3	+	4	5	+	2	+	+	-	0
50	F	MSA-C	2	+	12	14	+	2	+	+	+	0
64	F	MSA-C	2	+	14	24	+	4	+	+	+	0
62	F	MSA-C	3	+	14	18	+	3	+	+	+	0
64	M	MSA-C	3	+	10	11	+	2	+	+	+	0
64	F	MSA-C	3	+	30	12	+	4	+	-	-	+
52	F	MSA-C	8	+	33	22	+	5	+	+	+	+
53	F	MSA-C*	2	+	9	15	+	1	+	+	-	+
62	F	MSA-C	2	+	7	9	+	2	+	-	+	+
57	F	MSA-C	4	+	20	25	+	5	+	-	+	+
71	M	MSA-C	1	+	2	4	+	1	+	+	+	-
54	F	PD	10	-	NA				-	+	-	0
58	F	PD	3	-	NA				-	-	-	0
69	F	PD	10	-	NA				+	-	-	0
61	M	PD	6	-	NA				-	-	-	0
65	F	PD	10	-	NA				-	-	-	0
58	F	PD	4	-	NA				-	-	-	-
64	M	PD	8	-	NA				-	+	-	-
47	M	PSP	8	+	NA				-	-	-	0
69	M	PSP	3	+	NA				-	-	-	0
70	M	PSP	3	+	NA				-	-	-	0
69	F	PSP	3	+	NA				+	-	-	0
70	F	PSP-C	10	+	NA				-	-	-	0
67	M	PSP	4	+	NA				-	-	-	-

F, female; M, male; MSA-P, multiple system atrophy with predominant parkinsonism; MSA-C, multiple system atrophy with predominant cerebellar ataxia; PD, Parkinson's disease; PSP, progressive supranuclear palsy; PSP-C, progressive supranuclear palsy with predominant cerebellar ataxia; MRI, magnetic resonance imaging, including atrophy on MRI of putamen, middle cerebellar peduncle, pons, or cerebellum, -, absent; +, present; UMSARS, Unified Multiple System Atrophy Rating Scale (I. historical review of disease-related impairments; II. motor examination; III. autonomic examination, -, absent; +, present; IV. global disability scale); NA, not applicable.

*possible MSA-C.

†-, normal findings; +, abnormal findings.

‡ DET, detrusor; -, absent; +, present.

§ EUS, external urethral sphincter; -, absent; +, present; 0: not examined.

Transparent Methods

Patients

Forty-five patients (18 men, 27 women; age 60.6 ± 7.2 years) were enrolled consecutively from 2016 to 2018 with MSA (32 patients), PD (7 patients), or progressive supranuclear palsy (PSP) (6 patients) according to consensus criteria (Kalia and Lang, 2015; Litvan et al., 1996; Stefanova et al., 2009), respectively. In MSA, the phenotype was characterized by prevalently cerebellar signs in 19 patients and by parkinsonian signs in the remaining 13 patients. Disease severity was evaluated using Unified Multiple System Atrophy Rating Scale (UMSARS) (Low et al., 2015; Wenning et al., 2004). UMSARS Total is a sum of UMSARS Ⅰ and UMSARS Ⅱ. Demographic and clinical data are summarized in Table S1. At the time of enrollment, all subjects underwent clinical and electrophysiological evaluation as well as EUS and bladder biopsies at 3 sites: left wall, right wall, and triangle region (Figure 1J). Twenty subjects were also included in the study as controls (7 men, 13 women; age 58.5 ± 7.0 years). All biopsies were performed according to the outpatient procedures by experienced urologists in a prescriptive exam room. Cystoscopy was performed using standard cystoscope according to previously published procedures under local anesthesia with 1% xylocaine (Butros et al., 2015). The procedure was repeated until the EUS, left wall, right wall, and triangle region of bladder tissues were obtained. Samples were immediately fixed in 4% paraformaldehyde and kept at 4 °C for at least 2 days. All subjects provided informed consent for participation in the experiments. The study was executed with the approval of the Institutional Ethics Committees of the Zhengzhou University.

Urodynamic examination (UE) and external anal sphincter electromyography (EAS EMG) of patients

All human subjects underwent clinical and electrophysiological evaluation, including UE and EAS EMG, as previously described (Yamamoto et al., 2005; Yamamoto et al., 2014).

Animals

Male TgM83$^{+/-}$ expressing human A53T mutant α-Syn protein and male C57BL/6 as control mice were purchased from Nanjing Biomedical Research Institute of Nanjing University (Nanjing, China), and evaluated at the age of six to eight weeks. The hemizygous TgM83 mice expressed the human A53T α-Syn driven by the prion gene promoter (Giasson et al., 2002). C57BL/6 mice were chosen as the control mice because TgM83$^{+/-}$ mice were maintained on a mixed C57/C3H genetic background. Mice were kept in a near pathogen-free environment under standard conditions with food and water (21 °C, 12h/12h light-dark cycle). All experiments were conducted in accordance with the Guide for the Care and Use of Laboratory Animals. The protocols were approved by the Institutional Ethics Committees of the Zhengzhou University.

Surgery and retrograde tracing

To retrogradely label micturition reflex pathways, C57BL/6 and TgM83$^{+/-}$ mice were anesthetized with isoflurane inhalation (Prusiner et al., 2015), and 15 μl Fluoro-Gold (FG) (Fluorochrome, LLC, Denver, CO) was injected slowly into EUS or DET. Following the injections, the skin was sutured. After 14 days, mice were perfused as described before (Bácskai et al., 2014). The EUS or DET, pelvic ganglia, spinal cord and brain were removed and postfixed at 4 ℃ in a 30% sucrose solution containing 4% paraformaldehyde for at least 2 days. Serial transverse sections were cut at 20 μm using a freezing microtome (Leica CM1860 UV, Leica, Nussloch, Germany). Consecutive sections were collected, mounted, and cover-slipped with glycerol. Slides were then examined using an Olympus IX51 microscope equipped with epifluorescence.

α-Synuclein preformed fibrils (PFFs) preparation

Human α-Syn (S-1001, rPeptide) was resuspended in assembly buffer (20 mM Tris-HCl, 100 mM NaCl, pH 7.4) at concentration of 1 mg/ml. To obtain PFFs, the samples were placed in 2 ml sterile polypropylene tubes, sealed with parafilm, and agitated in a beaker with a magnetic stirrer (MS-H-Pro+, Scilogex, China) at 350 rpm for 7 days at 37 °C. After 7 days of incubation, the α-Syn fibrils were sonicated for 45 seconds using an ultrasonic cell disruptor at 10% of its peak amplitude (Scientz-IID, Ningbo, China). α-Syn fibrils were stored at -80 °C until use.

Transmission electron microscopy (TEM) imaging

The nature of the fibrillar α-Syn forms was assessed using Jeol 1400 (Jeol Ltd. Tokyo, Japan) TEM. First, a drop of fibrillar solution was transferred onto a carbon-coated 200-mesh grid and then negatively stained with 1% uranyl acetate. The images were recorded with Gatan Orius CCD camera (Gatan, Pleasanton, CA).

Modeling surgery

All injections were performed using a manual microinjector under an operating microscope. Mice were anesthetized with isoflurane inhalation and fixed in a supine position. After disinfection, mice were inoculated in the EUS with 15 μl α-Syn PFFs (48.89 ± 27.00 nm, 1 mg/ml) (Figure S1A-D) or phosphate buffered saline (PBS, Solarbio), or DET with 20 μl (1 mg/ml) α-Syn PFFs or PBS. The reason for selecting male mice is that the EUS boundary of male mice is clearer, making the injection more feasible. Following the injection, the exposed wound was sewn closed.

Immunohistochemical and double immunofluorescence staining

The paraffin-embedded tissues were cut into 4 μm thick sections with a Rotary Microtome (Leica RM2235, Leica, Nussloch, Germany). Immunohistochemistry and double-labeling immunofluorescence analysis were conducted as previously described by Luk et al. (Luk et al., 2012) using the following antibodies: phospho-α-synuclein (Ser 129) (mouse, Millipore, 1:800 or rabbit, Abcam, 1:600), α-synuclein filament (MJFR14) (rabbit, Abcam, 1:500), α-Syn aggregates (5G4) (mouse, Millipore, 1:800), ubiquitin (rabbit, Cell Signaling Technology, 1:400), Iba-1 (rabbit, Wako, 1:400), myelin basic protein (rabbit, Abcam, 1:900), neurofilament heavy polypeptide (mouse, Abcam, 1:600), anti-tyrosine hydroxylase (TH) (rabbit, Abcam, 1:600), glial fibrillary acidic protein (GFAP) (rabbit, Abcam, 1:600), microtubule-associated protein-2 (MAP-2) (rabbit, Abcam, 1:800), calbindin-D28k (rabbit, Abcam, 1:1000), Rhodamine Red™-X (RRX) AffiniPure donkey anti-mouse IgG (H+L) (donkey, Jackson ImmunoResearch, 1:400), Cy™2 AffiniPure donkey anti-rabbit IgG (H+L) (donkey, Jackson ImmunoResearch, 1:400). Cell nuclei were stained using Hoechst33258 (1:1000, Solarbio). Slides were coverslipped with

glycerol. Digital images were captured using Olympus IX51 microscope mounted with DP71 Olympus digital camera. Photoshop CS6 (Adobe Systems) was used to assemble montages.

We used 20 EUS-α-Syn PFFs TgM83$^{+/-}$ mice and 10 EUS-PBS TgM83$^{+/-}$ mice for statistical analysis of immunostaining. Calbindin-D28K-positive neurons and MAP-2-positive neurons were counted to evaluate the number of neurons. Mean optical density of MAP-2 was measured to evaluate the size of neurons using the ImageJ software (US National Institutes of Health). Mean optical density of MBP and GFAP was measured to evaluate demyelination and astrogliosis, respectively. The Pearson's correlation and the Mander's colocalization coefficients were measured to quantify the colocalization of ubiquitin with pα-Syn and TH using the ImageJ software. DET, EUS, pelvic ganglia, and serial coronal sections of the spinal cord, pons, midbrain, and cerebellum were analyzed, especially the representative sections of spinal cord (S1, L6, L2, T2), pons (Bregma -5.40 mm), midbrain (Bregma -3.16 mm), and cerebellum (Bregma -5.88 mm). The quantification and statistical analysis of the immunohistological results for each animal were conducted using the representative sections in a slide.

Tissue preparation

RIPA-insoluble fractions were prepared. Firstly, tissues were homogenized in TBS+ (50 mM Tris-HCl, pH 7.4, 175 mM NaCl; 5 mM EDTA, protease inhibitor cocktails). Then the homogenates were spun for 30 minutes at 120000 g and divided into soluble components and pellets. The soluble component refers to the supernatant after above step that does not contain α-Syn inclusions. The pallets contain most α-Syn inclusions. The pellets were subsequently extracted in TBS+ containing 1% Triton X-100, TBS+ containing 1M sucrose, and RIPA buffer, sequentially, and each extraction step was followed by centrifugation for 20 minutes at 12000g. After all these steps, we obtained the RIPA-insoluble pellets containing phosphorylated α-Syn (pα-Syn) inclusions. Then the RIPA-insoluble pellets were solubilized in 8 M urea/5% SDS for subsequent detection.

Sarkosyl-insoluble fractions were also prepared as previously described (Masuda-Suzukake et al., 2014). Firstly, tissues were homogenized in TBS+ (10 mM Tris-HCl, pH 7.4, 175 mM NaCl; 5 mM EDTA, protease inhibitor cocktails). Then the homogenates

were spun for 30 minutes at 120000g and divided into soluble components and pellets. The pellets were subsequently extracted in TBS+ containing 1% Triton X-100, and TBS+ containing 1% sarkosyl, sequentially, and each extraction step was followed by centrifugation for 20 minutes at 12000g. Then the sarkosyl-insoluble was solubilized in 30 mM Tris–HCl, pH 7.4 for subsequent detection.

Western blotting analysis

After mice were anesthetized and decapitated, the spinal cord and several brain regions such as PAG, RN, pons, and cerebellum were separated on a cold stage. The isolated mice tissues were then stored in liquid nitrogen for further treatment. The transferred polyvinylidene fluoride (PVDF) membranes for the Western blotting as previously described (Kohl et al., 2016) were incubated with phospho-α-synuclein (Ser 129) antibody (mouse, Millipore, 1:1200 or rabbit, Abcam, 1:1000). Forty-eight hours later, the membranes were washed in TBST (TBS with 0.1% Tween-20) and incubated with HRP-conjugated goat anti-mouse or goat anti-rabbit secondary antibodies for 2 hours at room temperature and visualized with enhanced chemiluminescence (Thermo Fisher Scientific). Proteins' densities on the blots were normalized against those of GAPDH. All immunoreactive bands from Western blotting analysis were quantified by pixel intensity using FluorChem 8900 software (Alpha Innotech, San Leandro, CA, USA). The relative pα-Syn level was measured by the ratio of the pixel intensity of the pα-Syn band to the pixel intensity of the corresponding GAPDH band.

EAS EMG

EAS EMG was carried out in all animals before injection for control groups and at correspondingly post-injection times to determine EAS denervation-reinnervation. Animals in each group underwent EAS EMG as follows (Aghaee-Afshar et al., 2009; Buffini et al., 2012; Healy et al., 2008; Lane et al., 2013): anesthesia was induced using isoflurane inhalation. Limb withdrawal to paw pinch and corneal reflexes of animals were observed to assess the level of anesthesia. After placing the animal supine, shaving the thigh, and establishing a ground connection, a disposable concentric 30-gauge needle electrode (Technomed Europe), which has a 25-mm length, 0.30-mm diameter, and

0.021-mm^2 recording area, was inserted at the 3 or 9 o'clock position of the anal orifice perpendicularly into the EAS from the perianal skin close to the mucocutaneous junction to a depth of approximately 1 to 2 mm. The point of the electrode insertion was adjusted under audio guidance until a permanent tonic activity was recorded, in order to ensure that the electrode has entered EAS. If the mouse discharged a fecal pellet during the recording process, a pair of forceps were used to gently clip it out. EMG was performed with an EMG monitoring machine (MEB-2306C, NIHON KOHDEN CORPORATION, Tokyo, Japan) at a sweep speed of 10 ms/div and a gain of 100 uv/div. Abnormal EAS EMGs were simultaneously visualized and recorded. EMG activity was quantified by frequency of abnormal EAS EMGs (fibrillation potentials, positive sharp waves, complex repetitive discharges (CRD), fasciculation potentials, myokymic discharges, and satellite potential) in each group (Daube and Rubin, 2009; Palace et al., 1997; Schwarz et al., 1997). Frequency of positive sharp waves in different groups was also separately analyzed.

Cystometry evaluations

All animals were subjected to cystometric experiment to evaluate their urinary function before injection and at corresponding time points of post-injection following the methods reported previously (Boudes et al., 2013; Fandel et al., 2016; Girard et al., 2012; Silva et al., 2015). The animal was put supine and the bladder was exposed via a lower midline abdominal incision under isoflurane anesthesia. A polyethylene catheter-50 (Clay-Adams, Parsippany, New Jersey, USA) was implanted into the apical bladder dome and secured in place with a 6/0 purse-string sutures (Ethicon, Noderstedt, Germany). We flushed the catheter with saline to ensure no leakage and then threaded it from neck to the lower back through the subcutaneous tunnel anchored to the neck skin, finally closed the abdominal wall and skin. Through a three-way tap, the bladder catheter was connected to an infusion pump (B. Braun Sharing Expertise, Germany) and a pressure transducer (AD Instruments, Castle Hill, New South Wales, Australia) coupled to a computerized BL-420S data acquisition and analysis system (Techman Soft, Chengdu, China) which amplified and recorded intravesical pressure from the pressure transducer. We applied a heating lamp and room-temperature saline to maintain the body

temperature of mice. Bladders were given a continuous infusion of 0.9% NaCl at a constant rate (20 μl/min) and after an equilibration period of 20-30 minutes, the intravesical pressure was recorded and voiding events were observed and noted for 30 minutes.

The following urodynamic parameters (Boudes et al., 2013; Fandel et al., 2016; Girard et al., 2012; Lee et al., 2013; Silva et al., 2015) were used for the current study: (1) Maximum voiding pressure (P_{max}; cmH_2O); (2) Basal bladder pressure (BBP; cmH_2O): the lowest bladder pressure during filling phase; (3) Amplitude (cmH_2O): P_{max} - BBP; (4) Bladder leak point pressure (BLPP; cmH_2O): intravesical pressure recorded at the first leaking/micturition point; (5) Threshold pressure (Pt; cmH_2O); (6) Nonvoiding contractions during filling phase (NVCs): rhythmic intravesical pressure rises (> 5 cmH_2O from baseline pressure) without any fluid leakage from the urethra; (7) Postvoid residual volume (PVR; ml): the remaining saline in the bladder collected and measured after stopping the infusion at the end of the final micturition cycle; (8) Maximum bladder capacity (MBC; ml): volume between the start of infusion and the BLPP; (9) Voided volume (VV; ml): MBC - PVR; (10) Intercontraction interval (ICI; s).

Behavioral test

To evaluate α-Syn PFFs-induced behavioral deficits, mice were assessed by the following tests. TgM83$^{+/-}$ and C57BL/6 mice were tested every 7 days starting from 2 mpi. Blinded experiments were performed to treatment group for all behavioral tests.

The motor behavioral scale (MBS)

MBS was used as Fernagut et al. previously reported (Fernagut et al., 2002). Higher score indicated higher disability and the maximum total score was 10. The total score was determined and used for the statistical analysis.

Rotarod test

Motor coordination was assessed following the method previously reported by Duclot et al. (Duclot et al., 2012) with modifications. In brief, a rotating rod (Rotarod YLS-4C; YiYan Science and Technology Development Co. Ltd., Shandong, China) was used. At each

time point, mice were placed on the rod rotating at 30 rpm. The latency to fall off the rotarod within the maximum time (180 seconds) was recorded, if a mouse stayed on the rod until the end of the 3 minutes, a time of 180 seconds was recorded. Mice received three trials per day with a 15-minute inter-trial interval. The mean latency to fall off the rotarod was statistically analyzed.

Open field test

To assess general activity, locomotion, and anxiety of the mice, the open field test system (Wuhan YiHong Sci. & Tech.Co. Ltd.) was applied. Mice were placed in the center of the open field (37.5 × 37.5 × 34.8 cm) and tested for 15 minutes at the same time of the day (6:00 p.m. to 9:00 p.m.). Activity was analyzed by the Anilab software version 5.10, registered version (Anilab Software & Instruments Co., Ltd., China). At the end of testing, the arena was cleaned with 75% alcohol to remove olfactory cues. The tests were performed in a dark room that was isolated from external noises and light during the test period. Total distance (cm), average speed (cm/s), and zone crossing were statistically analyzed.

Footprint test

The footprint test was performed to examine the gait of the mice. Paws of the mice were painted with water-soluble non-toxic paint of different colors (fore-paws in red and hind-paws in green). The animals were then allowed to walk along a restricted cardboard tunnel (50 cm long, 5 cm wide, 10 cm high) into an enclosed box and a sheet of white paper (42 cm long, 4.5 cm wide) was placed on the floor of the tunnel, and one set of footprints was collected for each animal. Three steps from the middle portion of each run were measured for four parameters (cm): (1) stride length (front and hind legs). (2) The front- and hind-base width. The mean of each set of values was statistically analyzed (Stefanova et al., 2005).

Beam walking test

Balance and bradykinesia were assessed with the method described before with modifications (Schafferer et al., 2016). The beams consisted of two different types of

wood (each measuring 80 cm long, one was 1.6 cm, and the other 0.9 cm wide) placed horizontally 50 cm above the floor, respectively. Two daily sessions of three trials were performed using the 1.6 cm width large beam during training. Mice were then tested using the 0.9 cm width beam. Mice were allowed to perform in three consecutive trials. The time for traversing 50 cm as well as the number of sideslip errors were recorded on each trial. The average traverse duration and average number of sideslip errors of the three trials were statistically analyzed.

Pole test

The pole test was performed to assess motor coordination and balance. A vertical gauze-taped pole (1 cm diameter, 50 cm height) with a small cork ball (3 cm diameter) at the top was applied. Mice were placed with their head upward right below the ball. The time taken to turn completely downward (T turn) and total time taken to reach the base of the pole with four paws (T total) were recorded. The maximum cutoff of total time to stop this test was 120 seconds. This test was performed three times for each mouse, while the average time was statistically analyzed (Zhou et al., 2016).

Statistical analysis

All statistical analyses of data were performed using SPSS 21.0 (IBM, Armonk, New York, USA) and Prism software 8.0 (GraphPad Software, La Jolla, CA). Data from immunohistochemistry, immunofluorescence, and negative-stained transmission electron micrographs were analyzed by ImageJ software (US National Institutes of Health). Characteristics of patients were presented as mean ± standard deviation (SD), statistical differences among groups of subjects were assessed using the one-way ANOVA. Histopathological parameters of mice were analyzed using Student's t test. Additionally, behavioral data and cystometry parameters of mice were presented as mean ± SD, employing Student's t test for comparison between two groups while one-way ANOVA for three when these data were distributed normally ($P > 0.05$ by Shapiro-Wilk test). Otherwise, the Mann-Whitney test was used for two groups versus Kruskal-Wallis test for three. Frequencies of abnormal EAS EMGs and positive sharp waves in different groups

were presented as mean ± standard error of mean (SEM) and statistically analyzed using the one-way ANOVA. P-values < 0.05 were considered to be statistically significant.

Supplemental References

Aghaee-Afshar, M., Rezazadehkermani, M., Asadi, A., Malekpour-Afshar, R., Shahesmaeili, A., and Nematollahi-mahani, S.N. (2009). Potential of human umbilical cord matrix and rabbit bone marrow-derived mesenchymal stem cells in repair of surgically incised rabbit external anal sphincter. Diseases of the colon and rectum *52*, 1753-1761.

Bácskai, T., Rusznák, Z., Paxinos, G., and Watson, C. (2014). Musculotopic organization of the motor neurons supplying the mouse hindlimb muscles: a quantitative study using Fluoro-Gold retrograde tracing. Brain structure & function *219*, 303-321.

Boudes, M., Uvin, P., Pinto, S., Voets, T., Fowler, C.J., Wenning, G.K., De Ridder, D., and Stefanova, N. (2013). Bladder dysfunction in a transgenic mouse model of multiple system atrophy. Movement disorders : official journal of the Movement Disorder Society *28*, 347-355.

Buffini, M., O'Halloran, K.D., O'Herlihy, C., O'Connell, P.R., and Jones, J.F. (2012). Comparison of the motor discharge to the voluntary sphincters of continence in the rat. Neurogastroenterology and motility : the official journal of the European Gastrointestinal Motility Society *24*, e175-184.

Butros, S.R., McCarthy, C.J., Karaosmanoglu, A.D., Shenoy-Bhangle, A.S., and Arellano, R.S. (2015). Feasibility and effectiveness of image-guided percutaneous biopsy of the urinary bladder. Abdominal imaging *40*, 1838-1842.

Daube, J.R., and Rubin, D.I. (2009). Needle electromyography. Muscle & nerve *39*, 244-270.

Duclot, F., Lapierre, M., Fritsch, S., White, R., Parker, M.G., Maurice, T., and Cavailles, V. (2012). Cognitive impairments in adult mice with constitutive inactivation of RIP140 gene expression. Genes, brain, and behavior *11*, 69-78.

Fandel, T.M., Trivedi, A., Nicholas, C.R., Zhang, H., Chen, J., Martinez, A.F., Noble-Haeusslein, L.J., and Kriegstein, A.R. (2016). Transplanted Human Stem Cell-Derived Interneuron Precursors Mitigate Mouse Bladder Dysfunction and Central Neuropathic Pain after Spinal Cord Injury. Cell stem cell *19*, 544-557.

Fernagut, P.O., Diguet, E., Stefanova, N., Biran, M., Wenning, G.K., Canioni, P., Bioulac, B., and Tison, F. (2002). Subacute systemic 3-nitropropionic acid intoxication induces a distinct motor disorder in adult C57Bl/6 mice: behavioural and histopathological characterisation. Neuroscience *114*, 1005-1017.

Giasson, B.I., Duda, J.E., Quinn, S.M., Zhang, B., Trojanowski, J.Q., and Lee, V.M. (2002). Neuronal alpha-synucleinopathy with severe movement disorder in mice expressing A53T human alpha-synuclein. Neuron *34*, 521-533.

Girard, B.M., Tompkins, J.D., Parsons, R.L., May, V., and Vizzard, M.A. (2012). Effects of CYP-induced cystitis on PACAP/VIP and receptor expression in micturition pathways and bladder function in mice with overexpression of NGF in urothelium. Journal of molecular neuroscience : MN *48*, 730-743.

Healy, C.F., O'Herlihy, C., O'Brien, C., O'Connell, P.R., and Jones, J.F. (2008). Experimental models of neuropathic fecal incontinence: an animal model of childbirth injury to the pudendal nerve and external anal sphincter. Diseases of the colon and rectum *51*, 1619-1626; discussion 1626.

Kalia, L.V., and Lang, A.E. (2015). Parkinson's disease. Lancet (London, England) *386*, 896-912.

Kohl, Z., Ben Abdallah, N., Vogelgsang, J., Tischer, L., Deusser, J., Amato, D., Anderson, S., Muller, C.P., Riess, O., Masliah, E.*, et al.* (2016). Severely impaired hippocampal neurogenesis associates with an early serotonergic deficit in a BAC alpha-synuclein transgenic rat model of Parkinson's disease. Neurobiology of disease *85*, 206-217.

Lane, F.L., Jacobs, S.A., Craig, J.B., Nistor, G., Markle, D., Noblett, K.L., Osann, K., and Keirstead, H. (2013). In vivo recovery of the injured anal sphincter after repair and injection of myogenic stem cells: an experimental model. Diseases of the colon and rectum *56*, 1290-1297.

Lee, Y.S., Lin, C.Y., Jiang, H.H., Depaul, M., Lin, V.W., and Silver, J. (2013). Nerve regeneration restores supraspinal control of bladder function after complete spinal cord injury. The Journal of neuroscience : the official journal of the Society for Neuroscience *33*, 10591-10606.

Litvan, I., Agid, Y., Calne, D., Campbell, G., Dubois, B., Duvoisin, R.C., Goetz, C.G., Golbe, L.I., Grafman, J., Growdon, J.H.*, et al.* (1996). Clinical research criteria for the diagnosis of progressive supranuclear palsy (Steele-Richardson-Olszewski syndrome): report of the NINDS-SPSP international workshop. Neurology *47*, 1-9.

Low, P.A., Reich, S.G., Jankovic, J., Shults, C.W., Stern, M.B., Novak, P., Tanner, C.M., Gilman, S., Marshall, F.J., Wooten, F., *et al.* (2015). Natural history of multiple system atrophy in the USA: a prospective cohort study. The Lancet Neurology *14*, 710-719.

Luk, K.C., Kehm, V.M., Zhang, B., O'Brien, P., Trojanowski, J.Q., and Lee, V.M. (2012). Intracerebral inoculation of pathological alpha-synuclein initiates a rapidly progressive neurodegenerative alpha-synucleinopathy in mice. The Journal of experimental medicine *209*, 975-986.

Masuda-Suzukake, M., Nonaka, T., Hosokawa, M., Kubo, M., Shimozawa, A., Akiyama, H., and Hasegawa, M. (2014). Pathological alpha-synuclein propagates through neural networks. Acta neuropathologica communications *2*, 88.

Palace, J., Chandiramani, V.A., and Fowler, C.J. (1997). Value of sphincter electromyography in the diagnosis of multiple system atrophy. Muscle & nerve *20*, 1396-1403.

Prusiner, S.B., Woerman, A.L., Mordes, D.A., Watts, J.C., Rampersaud, R., Berry, D.B., Patel, S., Oehler, A., Lowe, J.K., Kravitz, S.N., *et al.* (2015). Evidence for α-synuclein prions causing multiple system atrophy in humans with parkinsonism. Proc Natl Acad Sci U S A *112*, E5308-5317.

Schafferer, S., Khurana, R., Refolo, V., Venezia, S., Sturm, E., Piatti, P., Hechenberger, C., Hackl, H., Kessler, R., Willi, M., *et al.* (2016). Changes in the miRNA-mRNA Regulatory Network Precede Motor Symptoms in a Mouse Model of Multiple System Atrophy: Clinical Implications. PloS one *11*, e0150705.

Schwarz, J., Kornhuber, M., Bischoff, C., and Straube, A. (1997). Electromyography of the external anal sphincter in patients with Parkinson's disease and multiple system atrophy: frequency of abnormal spontaneous activity and polyphasic motor unit potentials. Muscle & nerve *20*, 1167-1172.

Silva, R.B., Sperotto, N.D., Andrade, E.L., Pereira, T.C., Leite, C.E., de Souza, A.H., Bogo, M.R., Morrone, F.B., Gomez, M.V., and Campos, M.M. (2015). Spinal blockage of P/Q- or N-type voltage-gated calcium channels modulates functional and symptomatic changes related to haemorrhagic cystitis in mice. British journal of pharmacology *172*, 924-939.

Stefanova, N., Bucke, P., Duerr, S., and Wenning, G.K. (2009). Multiple system atrophy: an update. The Lancet Neurology *8*, 1172-1178.

Stefanova, N., Reindl, M., Neumann, M., Haass, C., Poewe, W., Kahle, P.J., and Wenning, G.K. (2005). Oxidative stress in transgenic mice with oligodendroglial alpha-synuclein overexpression replicates the characteristic neuropathology of multiple system atrophy. The American journal of pathology *166*, 869-876.

Wenning, G.K., Tison, F., Seppi, K., Sampaio, C., Diem, A., Yekhlef, F., Ghorayeb, I., Ory, F., Galitzky, M., Scaravilli, T., *et al.* (2004). Development and validation of the Unified Multiple System Atrophy Rating Scale (UMSARS). Movement disorders : official journal of the Movement Disorder Society *19*, 1391-1402.

Yamamoto, T., Sakakibara, R., Uchiyama, T., Liu, Z., Ito, T., Awa, Y., Yamamoto, K., Kinou, M., Yamanishi, T., and Hattori, T. (2005). When is Onuf's nucleus involved in multiple system atrophy? A sphincter electromyography study. Journal of neurology, neurosurgery, and psychiatry *76*, 1645-1648.

Yamamoto, T., Sakakibara, R., Uchiyama, T., Yamaguchi, C., Ohno, S., Nomura, F., Yanagisawa, M., Hattori, T., and Kuwabara, S. (2014). Time-dependent changes and gender differences in urinary dysfunction in patients with multiple system atrophy. Neurourology and urodynamics *33*, 516-523.

Zhou, T., Zu, G., Zhang, X., Wang, X., Li, S., Gong, X., Liang, Z., and Zhao, J. (2016). Neuroprotective effects of ginsenoside Rg1 through the Wnt/beta-catenin signaling pathway in both in vivo and in vitro models of Parkinson's disease. Neuropharmacology *101*, 480-489.